HHS Public Access

Author manuscript

Nat Struct Mol Biol. Author manuscript; available in PMC 2014 May 01.

Published in final edited form as:

Nat Struct Mol Biol. 2013 November ; 20(11): 1310–1317. doi:10.1038/nsmb.2687.

Structural insights into H+-coupled multidrug extrusion by a MATE transporter

Min Lu, **Martha Radchenko**, **Jindrich Symersky**, **Rongxin Nie**, and **Yi Guo**

Department of Biochemistry and Molecular Biology, Rosalind Franklin University of Medicine and Science, North Chicago, IL 60064, USA

Abstract

Multidrug and toxic compound extrusion (MATE) transporters contribute to multidrug resistance by coupling the efflux of drugs to the influx of Na^+ or H^+. Known structures of Na^+-coupled, extracellular-facing MATE transporters from the NorM subfamily revealed twelve membrane-spanning segments related by a quasi-twofold rotational symmetry and a multidrug-binding cavity situated near the membrane surface. Here we report the crystal structure of an H^+-coupled MATE transporter from *Bacillus halodurans* and the DinF subfamily at 3.2 Å-resolution, unveiling a surprisingly asymmetric arrangement of twelve transmembrane helices. We also identified a membrane-embedded substrate-binding chamber by combining crystallographic and biochemical analyses. Our studies further suggested a direct competition between H^+ and substrate during DinF-mediated transport, and how a MATE transporter alternates between its extracellular- and intracellular-facing conformations to propel multidrug extrusion. Collectively, our results demonstrated hitherto unrecognized mechanistic diversity among MATE transporters.

Integral membrane proteins dubbed “multidrug transporters” can extrude structurally and chemically distinct drugs from cells, giving rise to multidrug resistance, a major obstacle to the effective treatment of infectious diseases and human cancers[1,2]. To date, five classes of multidrug transporters have been identified[1], including the ABC (ATP-binding cassette), MATE (multidrug and toxic compound extrusion), MFS (major facilitator superfamily), RND (resistance-nodulation-division) and SMR (small multidrug resistance) transporter families. Aside from the primary ABC transporters that are powered by ATP hydrolysis, most multidrug transporters are secondary transporters that catalyze drug extrusion typically by exploiting the transmembrane H^+ gradient.

Correspondence should be addressed to M.L. (min.lu@rosalindfranklin.edu).

Accession codes. Coordinates and structure factors have been deposited into the Protein Data Bank under the accession codes 4LZ6 and 4LZ9.

Note: Supplementary information is available in the online version of the paper.

AUTHOR CONTRIBUTIONS

M.L. conceived the project. M.L. and Y.G. expressed, purified and crystallized the proteins. M.L. and J.S. collected and analyzed X-ray diffraction data. M.R., R.N. and M.L. conducted mutagenesis and functional studies. M.L. wrote the manuscript.

COMPETING FINANCIAL INTERESTS

The authors declare no competing financial interests.

The ~900 MATE transporters can be classified into the NorM, DinF (DNA-damage-inducible protein F) and eukaryotic subfamilies based on amino-acid sequence similarity[3–5]. Members of the NorM and DinF branches can utilize either the Na^+ or H^+ electrochemical gradient to extrude polyaromatic and cationic drugs[6–10], whereas eukaryotic MATE transporters are typically H^+-coupled[11–13]. Although the NorM and DinF subfamilies both have eubacterial and archeal members, they share rather low amino-acid sequence homology.

The structures of several Na^+-coupled NorM transporters had been determined to 3.5–3.65 Å resolutions, including those from *Vibrio cholerae* (NorM-VC)[14] and *Neisseria gonorrhoeae* (NorM-NG)[15], which revealed a common protein fold characterized by a pseudo-twofold rotational symmetry within the membrane-spanning core domain composed of twelve transmembrane helices (TM1-TM12). The Rb^+-bound, substrate-free NorM-VC structure[14] suggested the location of the Na^+-binding site within the carboxyl domain (TM7-TM12), whereas the structures of NorM-NG bound to various substrates unveiled a periplasm-facing drug-binding site located at the interface between the amino (TM1-TM6) and carboxyl halves of the protein[15]. Furthermore, the NorM-NG structures suggested that substrate and cation interact with distinct subsets of amino acids, implying an antiport mechanism mediated by Na^+-coupled rearrangement of transmembrane helices[15].

In the NorM structures, however, the interface between the amino and carboxyl domains always opens into the periplasm, i.e., extracellular-facing states. As such, the mechanistic principles that define the interconversion between the extracellular- and intracellular-facing conformations, which lies at the heart of multidrug extrusion, remain enigmatic[16, 17]. Furthermore, although DinF proteins had been well-documented to render cells resistant to various cytotoxic chemicals[18–21], they apparently lack the cation-binding motif comprising one aromatic and two acidic amino acids[15], which is indispensible for the transport function of NorM and eukaryotic MATE transporters[22,23]. To resolve such vexing issues, we set out to investigate the mechanism of DinF transporters.

RESULTS

Functional characterization of DinF-BH

In this work, we assessed the functionality of a DinF protein from *Bacillus halodurans* (DinF-BH). We observed that DinF-BH conferred cellular resistance towards diverse cytotoxic compounds including ethidium, rhodamine 6G (R6G) and tetraphenylphosphonium (TPP) (Supplementary Table 1), which are cationic at physiological pH. Moreover, our drug transport assays showed that DinF-BH reduced the R6G fluorescence by extruding drugs in the presence of an inwardly directed H^+ gradient or diethanolamine, a membrane-permeable amine that can stimulate H^+-coupled antiporter activity by increasing cytoplasmic pH[24] (Fig. 1a). By contrast, neither the H^+ gradient nor diethanolamine triggered NorM-NG mediated R6G efflux in *E. coli*. As NorM-NG functions as a Na^+-coupled multidrug transporter[8,15], these results suggested that recombinant DinF-BH was expressed as a functional “multidrug” transporter to effect H^+-coupled drug efflux.

To confirm the H^+-coupling, we analyzed H^+ flux in a drug-H^+ antiport assay by measuring the changes in fluorescence quenching in everted membrane vesicles[9,24,25]. We found that the addition of a substrate, TPP, elicited efflux of H^+ in DinF-BH containing membrane vesicles and caused fluorescence dequenching (Fig. 1b). By contrast, everted membrane vesicles containing NorM-NG showed no response to TPP. Furthermore, we examined the cation dependence of DinF-BH mediated transport by measuring drug accumulation levels in bacteria[8]. As a comparison, the accumulation of drugs in cells expressing Na^+-coupled NorM-NG was lower in the presence of Na^+ than that of K^+ (Fig. 1c). By contrast, we observed no measurable difference in drug accumulation in cells expressing DinF-BH when Na^+ was replaced by K^+. Altogether, our data supported DinF-BH as an H^+- rather than Na^+-coupled transporter.

Structure overview of DinF-BH

To gain further mechanistic insights into DinF-BH mediated transport, we determined its crystal structure at 3.2 Å-resolution by combining molecular replacement and MIRAS (multiple isomorphous replacement and anomalous scattering) phasing (Supplementary Fig. 1, Table 1). As shown in Fig. 2 and Supplementary Fig. 2, each asymmetric unit revealed one DinF-BH molecule, which contains twelve membrane-spanning helices (TM1-TM12) with both amino- and carboxyl-termini facing the cytoplasm, as is typical for MATE transporters of known structure[14,15].

In both NorM-VC and NorM-NG, TM1-TM6 is structurally related to TM7-TM12 around a pseudo-twofold rotational axis running approximately perpendicular to the membrane plane. The structures of the two domains in NorM-NG could be superimposed onto each other with an rms deviation of 2.39 Å for 142 common Cα positions. By contrast, structural superimposition of the two domains in DinF-BH yielded an rms deviation of 3.30 Å for 138 common Cα positions. The most notable difference between the two halves of DinF-BH is localized in the extracellular halves of TM7-TM8 (residues 253–288) and their counterparts in TM1-TM2 (Supplementary Fig. 2). If those residues were excluded, the rms deviation could be lowered to 2.50 Å over 108 Cα atoms. Compared with TM1 and TM2, both TM7 and TM8 are more “kinked” near their midsections, which appear to be induced by P247 and P291, respectively. In order to align closely with their counterparts in TM1 and TM2, the extracellular halves of TM7-TM8 in DinF-BH need to tilt 20° relative to the membrane normal in order to “straighten” the kinks.

Wide crevice within the carboxyl domain

The structural “asymmetry” of DinF-BH creates a wide crevice within its carboxyl domain, which is open to both the periplasm and outer membrane leaflet (Fig. 2a,b and Supplementary Fig. 2). This crevice effectively separates the carboxyl domain into two layers of helices, with TM7 and TM8 aligned in one and TM9 to TM12 in the other. This separation suggests that substantial structural rearrangement in DinF-BH is needed to form a similar cation-binding site to that of NorM transporters[14], which requires close interhelical packing between TM7-TM8 and TM9-TM12 (Fig. 2c,d). Notably, all DinF transporters lack the cation-binding motif that is conserved in the NorM branch, which is exemplified by E261 (TM7), Y294 (TM8) and D377 (TM10) in NorM-NG[15]. The absence of conserved

protonable amino acids in DinF-BH therefore implies a cation-binding site distinct from that of NorM transporters.

Rather than interacting closely with TM9-TM12 as in NorM transporters, the extracellular halves of TM7 and TM8 in DinF-BH bend back and pack snugly against TM2 and TM1, respectively (Fig. 2b). In so doing, TM1-TM8 collectively form an internal “chamber” that can potentially shelter encapsulated substrate. The interior of the chamber is populated with numerous hydrophobic amino acids, whose bulky side chains can insulate the bound substrate from the outside environment. Additionally, TM7 and TM8 define a lateral fenestration through which H^+ from the solvent-filled crevice can gain access to the internal chamber (Supplementary Fig. 2). At the widest point within the membrane bilayer, the fenestration is 10 Å wide, which could also allow substrate to slide from sideways out of the chamber and into the crevice. The access to the chamber from the cytoplasm side, however, is blocked by highly ordered protein structure.

Identification of the substrate-binding site

To locate the drug-binding site, we soaked cationic substrate R6G into the DinF-BH crystals and determined the structure to 3.7 Å-resolution by combining molecular replacement and MIRAS phasing (Supplementary Fig. 3, Table 2). The experimental phases improved the observable-to-parameter ratio during structure refinement, and allowed us to objectively examine possible, drug-induced protein conformational changes. Furthermore, the experimental electron density map revealed prominent electron density feature within the internal chamber that well-matched the bound substrate (Fig. 3). This density feature strictly depended on the incubation with R6G, as we had never observed such density in the apo form. Importantly, the well-resolved electron density enabled us to define the orientation of the bound substrate with confidence (Fig. 3b and Supplementary Fig. 3).

Moreover, we calculated anomalous difference Fourier maps using data collected on crystals incubated in solutions containing tetraphenylarsonium, a TPP analog[26] and also a substrate for DinF-BH (Supplementary Table 1). A strong anomalous peak pinpointed the position of the arsenic atom (corresponding to the phosphorus atom in TPP) and spatially coincided with R6G (Fig. 3b). This finding provided additional unbiased support for the identification of the “multidrug”-binding site. Overall, there was little structural difference between the apo and drug-bound protein (rms deviation ~0.5 Å for 446 Cα positions), which was supported by the experimental maps calculated for both the apo and R6G-soaked crystal forms (Supplementary Fig. 3). As the substrate-binding site is accessible to the periplasm via the solvent-exposed crevice, we suggest that both structures represent an extracellular-facing DinF-BH.

Deeply nestled within the transmembrane core domain, the substrate-binding site of DinF-BH contrasts markedly with that of NorM-NG[15], which is near the membrane-periplasm interface (Supplementary Fig. 4). Within the drug-binding chamber of DinF-BH, amino-acid side-chains project from TM1, TM2, TM4, TM5, TM6 and TM8 towards R6G (Fig. 3c). In contrast to NorM-NG, which employs only a few hydrophobic residues in drug-binding[15], copious close-range contacts between DinF-BH and R6G are mediated by hydrophobic amino acids, five of which are aromatic. Specifically, M33, I44 (TM1), V56, F60, M63,

M67 (TM2), F150, F154 (TM4), M173 (TM5), M286 (TM8) all make hydrophobic interactions with R6G; whereas Y36, N37, D40 (TM1), Y139 (TM4) and Q206 (TM6) make either charge-dipole or charge-charge interactions with the bound substrate. Among them, D40 is highly conserved within the DinF subfamily and makes the only ionic contacts with R6G. By contrast, NorM-NG utilizes four acidic amino acids to bind R6G[15].

Functional importance of the substrate-binding site

To verify the biological importance of the observed interactions between DinF-BH and R6G, we mutated all the drug-binding amino acids and explored the functional consequences by conducting drug resistance assays (Fig. 4a). The results revealed that DinF-BH variants M33A, D40A, D40N, D40K, I44A, V56A, M67A, M173A, I200A, Q206A and M286A were all unable to relieve the drug sensitivity of bacteria, which was most likely due to their impaired transport function, because membranes bearing those mutant proteins showed no response to TPP in the drug-H^+ antiport assay. By contrast, DinF-BH variants Y36A, N37A, F60A, M63A, Y139A, F150A and F154A retained their ability to confer drug resistance (Fig. 4a). Altogether, our data ascertained that the internal chamber harbors a functionally relevant substrate-binding site and amino-acid side-chains at positions M33, D40, I44, V56, M67, M173, Q206 and M286 play pivotal roles in multidrug transport.

Notably, the key electrostatic component of R6G binding is via D40, which appears to play a critical role in selecting for positively charged substrates. Furthermore, D40 is a prime candidate for the cation-binding (protonation) site in DinF-BH. Located within a membrane-embedded chamber that harbors numerous hydrophobic amino acids, D40 is effectively shielded from the solvent-exposed crevice by TM7 and TM8 (Supplementary Fig. 4). Consistent with this arrangement, the side-chain carboxylate of D40 has a calculated pKa of 7.4 (ref. 27) and can conceivably undergo cycles of protonation and deprotonation as substrates are shuttled through the transporter *in vivo*[25,28].

By contrast, the membrane-embedded, drug-binding aspartate in NorM-NG (NorM-NG^{D41}) is located in a central cavity that is populated with acidic and polar amino-acid side-chains, and only modestly shielded from the periplasm by extracellular loops[15] (Supplementary Fig. 4). As a consequence, NorM-NG^{D41} has a calculated pKa of 5.8, which is lower than that of D40 in DinF-BH. Apparently, the arrangement of TM7 and TM8, as well as hydrophobicity of the substrate-binding sites in NorM-NG and DinF-BH, perturb the pKa of side-chain carboxylates to different extents, rendering D40 in DinF-BH chemically more suitable than NorM-NG^{D41} to serve as a protonation site at physiological pH. Since the DinF-BH crystals were obtained at pH8.5, it follows that our structures portray a deprotonated transporter.

Direct competition between drug and H^+

In support of D40's role as a key cation-binding residue, a protonation-mimetic mutation D40N, which presumably "locks" D40 in its protonated state, abrogated the ability of DinF-BH to confer drug resistance or to catalyze drug-H^+ exchange (Fig. 4b). Indeed, the D40N mutation drastically reduced the R6G binding affinity of DinF-BH (Fig. 4c). Additionally, treatment of DinF-BH with dicyclohexylcarbodiimide, a chemical that reacts with

protonated carboxyls in a hydrophobic environment[25], abolished the binding of R6G to DinF-BH.

Therefore, membrane-embedded acidic amino acid(s) appears to be essential for the transport function of DinF-BH. Most likely, this is because substrate and H^+ compete for D40 during multidrug extrusion. In accord with this competition, H^+ exerts inhibitory effects on R6G binding to DinF-BH, which could be abrogated by mutation D40N (Supplementary Fig. 4). By contrast, R6G binding to NorM-NG was insensitive to the H^+ concentrations, consistent with NorM-NG being a Na^+- rather than H^+-coupled transporter[8]. Furthermore, analysis of the pH-dependent R6G binding to DinF-BH revealed a pKa of ~7.2 for the competing H^+, which likely reflects the effects of D40 protonation on R6G binding, because H^+ could no longer interfere with the binding when D40 was replaced by an non-protonatable residue.

To confirm the direct competition between drug and H^+, we studied the drug-triggered H^+-release by using a fluorescent pH indicator[25,28]. As shown in Fig. 4d, addition of substrate triggered a stoichiometric (1:1) release of H^+ from DinF-BH. Since our structure indicated a single drug-binding site in DinF-BH (Fig. 3b), it follows that each substrate induces the release of a single H^+ from the transporter. Furthermore, mutation D40N abolished the ability of DinF-BH to release H^+ upon drug-binding (Fig. 4e), arguing that substrate triggers H^+ release by directly binding to D40. Taken together, our data are consistent with a direct competition between H^+ and drug, which is essential for the antiport function of DinF-BH. This ligand-sharing arrangement of cation- and substrate-binding sites is distinct from that of NorM-NG, in which substrate and cation interact with completely different subsets of amino acids[15].

Modeling the intracellular-facing conformation

Although our DinF-BH structures represent an extracellular-facing conformation of the transporter, we reasoned that the conformation of the extracellular halves of TM7 and TM8 reflects that in the intracellular-facing state, as they pack snugly against TM1 and TM2, thereby occluding the interface between the amino and carboxyl domains from the periplasm (Fig. 2b). We also anticipated that in the intracellular-facing DinF-BH, TM9-TM12 interact closely with TM7 and TM8, so that the wide crevice in the carboxyl domain can be sealed off to occlude the drug-binding site from the periplasm.

Based on these considerations, we generated an intracellular-facing model of DinF-BH (Fig. 5a). Without causing any obvious steric clashes, we rotated the cytoplasmic halves of TM7 and TM8, as well as TM9-TM12, by 20° relative to the rest of the protein. Notably, the rotation of TM9-TM12 collapsed the solvent-exposed crevice within the carboxyl domain, whereas that of TM7 and TM8 exposed the drug-binding site towards the cytoplasm (Fig. 5b). In so doing, the intracellular and extracellular halves of both TM7 and TM8 moved to different extents, rather than tilting as rigid-bodies. Effectively, this motion straightened the kinks in TM7 and TM8, which may be well-accommodated by the proline (P247 and P291) and glycine (G245 and G294) residues, as well as the 18-residue intracellular loop between TM6 and TM7.

Functional importance of TM7 and TM8 in DinF-BH

We further predicted that the perturbation of the intracellular transport pathway in DinF-BH would affect the conformational changes and/or substrate binding required for drug translocation, thereby altering the transport function, as often happens in membrane transporters[29–31]. Henceforth, we individually mutated eleven amino acids along the intracellular transport path in DinF-BH, and probed their impact on the transport function by conducting drug resistance assays (Fig. 5c, d). We found that mutations of L22, V241, V244, F249 and Q297 all impaired the ability of DinF-BH to confer cellular resistance to drugs. In keeping with these results, those mutations also abolished the drug-H^+ exchange activity of DinF-BH in everted membrane vesicles.

To delve more deeply into the functional roles of those amino acids, we purified mutant proteins L22A, V241A, V244A, F249A and Q297A, which were expressed to the same level as the wild type protein, and found to be well-folded based on gel filtration chromatography. We then carried out the fluorescence-based H^+-release assay and observed that all the mutant proteins released a stoichiometric H^+ upon TPP binding as the wild type protein (Fig. 4d). Altogether, our analyses indicated that L22, V241, V244, F249 and Q297 play crucial roles in the transport function, as single alanine substitutions of those amino acids had no deleterious consequence on the expression or solution behavior of DinF-BH. Apparently, drug-induced H^+-release was not affected by those mutations, implying that those amino-acid side-chains participate in the interconversion between the intracellular- and extracellular conformations rather than directly binding substrates. Notably, V241, V244 and F249 are located in the intracellular half of TM7, whereas Q297 lies in that of TM8. Therefore, our data showed high concordance with the putative structural rearrangement of TM7 and TM8 during the transition from the extracellular- to intracellular-facing state (Fig. 5a,b).

Functional Importance of TM7 and TM8 in NorM-NG

To make greater inroads into the MATE-mediated transport, we used the intracellular-facing model of DinF-BH as a template to map the intracellular transport route in NorM-NG, given their structural similarity (rms deviation of 2.97 Å for 279 common Cα positions). We generated twelve NorM-NG mutants, each with a mutation targeting a solvent-exposed amino acid along the cytoplasm-facing transport route (Supplementary Fig. 5). We then examined the function of those NorM-NG variants by utilizing the drug resistance assay. As shown in Supplementary Fig. 5, mutations Q34A, I68A, I254A, Y258A, M295A, T305A and R388A abolished the ability of NorM-NG to relieve the sensitivity of bacteria towards drugs. Furthermore, those mutations severely impaired the R6G efflux activity of NorM-NG.

Among them, I254, Y258, M295 and T305 are located within the cytoplasmic portions of TM7 and TM8 in NorM-NG (Supplementary Fig. 5). These findings thus further substantiated the intracellular halves of TM7 and TM8 as functionally important. Additionally, TM7 and TM8 in NorM-NG had been implicated in the Na^+-coupled conformational changes during drug export[15]. Collectively, our data suggested that TM7 and TM8 play important roles in the transport function of NorM-NG and DinF-BH, which is

consistent with a similar intracellular transport pathway among those prokaryotic MATE homologues.

Proposed antiport mechanism

With both the extracellular- and intracellular-facing models in hand, we can now describe the major steps during the transport cycle for DinF-BH (Fig. 6). In our working hypothesis, H^+ disrupts drug-binding by competing directly for D40 in the extracellular-facing, drug-bound transporter (state I). The resulting extracellular-facing, protonated transporter (state II) then switches to the intracellular-facing and protonated state, which involves a 20° rotation of the cytoplasmic halves of TM7-TM8 as well as TM9-TM12 relative to the rest of the protein (state III). This motion, probably driven by the thermal energy, enables the transporter to capture new substrate from the cytoplasm. Drug binding then triggers deprotonation of the transporter by directly competing for D40 (state IV). The intracellular-facing, drug-bound transporter can then return to the extracellular-facing, drug-bound state to begin another transport cycle (state I).

Importantly, our results suggested a key difference between NorM-NG and DinF-BH in the mode of interaction between the substrate and counter-transported cation. In NorM-NG, cation- and substrate-binding sites are spatially well-separated, which implies that Na^+ induces drug extrusion through an indirect competition mechanism, i.e., via protein conformational changes[15] (Supplementary Fig. 6). By contrast, in DinF-BH, H^+ most likely triggers drug release by competing for a substrate-binding amino acid (D40), during which no substantial rearrangement of transmembrane helices would be necessary (Fig. 6). This mechanistic disparity hints at striking functional diversity between NorM and DinF transporters despite their overall structural similarity, thereby challenging the routinely made assumption that all MATE proteins share a common antiport mechanism[14,32].

DISCUSSION

Structural diversity within the DinF branch

After we had determined the structures of DinF-BH, the crystal structures of an H^+-coupled, extracellular-facing DinF transporter from *Pyrococcus furiosus* (pfMATE) were reported at 2.1–3.0 Å resolutions[32]. In particular, the authors determined the pfMATE structures at both high (7.0–8.0) and low (6.0–6.5) pH, both of which resemble that of the substrate-free NorM-VC[14] and are largely identical except that TM1 is more bent in the low pH structure. Moreover, the authors identified the binding site for a norfloxacin analog (Br-NRF) and proposed an antiport mechanism wherein the protonation of D41 (the cation-binding site) in pfMATE triggers the bending of TM1 to extrude drugs.

Both DinF-BH and pfMATE contain a conserved aspartate in TM1 (DinF-BH^{D40} and pfMATE^{D41}), and both share appreciable amino-acid sequence similarity (27% identity). As a comparison, DinF-BH bears only 11% amino-acid sequence identity to NorM-NG. Unlike DinF-BH^{D40}, however, pfMATE^{D41} is readily accessible from a solvent-filled cavity that is formed between the pseudo-symmetric TM1-TM6 and TM7-TM12 (Supplementary Fig. 7). As a result, in both the high and low pH structures, pfMATE^{D41} has a calculated pKa of

<3.6 (ref. 27), which is substantially lower than that of DinF-BH^{D40}. The structural and chemical differences of this conserved, protonatable amino acid between DinF-BH and pfMATE, if real, would imply a divergent evolution of the two transporters.

Moreover, there are critical differences between the antiport mechanisms proposed for pfMATE and DinF-BH. In pfMATE, the coupling between H^+ and substrate was suggested to be mediated by the bending or straightening of TM1, and allosteric in nature[32]. In DinF-BH, however, we contend that H^+ and substrate compete for a shared binding site, i.e., direct coupling. We also argue that TM7 and TM8 in DinF-BH shield D40 from the bulk solvent so that its side-chain carboxylate can serve as a protonation site *in vivo*.

Different substrate-binding sites

Besides their cation-binding sites, the substrates-binding sites also differ significantly among DinF-BH, NorM-NG and pfMATE (Supplementary Fig. 7). Our studies herein revealed a multidrug-binding chamber in DinF-BH that harbors numerous hydrophobic amino acids, including three phenylalanines and two tyrosines. The largely hydrophobic substrate-binding chamber in DinF-BH markedly contrasts with the drug-binding cavity in NorM-NG, which is comprised mainly of acidic and polar amino acids[15]. In NorM-NG, most of the close-range interactions between the protein and bound substrate are mediated by charge-charge and charge-dipole interactions, and only one aromatic amino acid makes direct contacts with the bound substrate.

In DinF-BH, by contrast, D40 makes the only ionic contacts with the bound substrate. Given the low dielectric constant within the transmembrane domain, the loss of the electrostatic attraction mediated by D40 should considerably weaken substrate-binding. Apparently, the hydrophobic drug-binding chamber in DinF-BH provides a suitable chemical environment for D40 to serve dual function in drug transport: substrate binding and protonation. Despite those differences, the drug-binding sites in NorM-NG and DinF-BH both involve the amino and carboxyl domains, and both exhibit a surplus of negative charge (Supplementary Fig. 7), the latter of which is consistent with their preferences for transporting cationic substrates.

Notably, the drug-binding site observed in pfMATE is formed exclusively within the amino domain[32], dominated by polar amino acids and exhibits a striking surplus of positive charge (Supplementary Fig. 7). The different locations and surface charges of the substrate-binding sites seen among the three MATE transporters were perhaps partly due to that chemically distinct substrates had been used in those studies. As such, the current study adds to the burgeoning body of data that point to hitherto unsuspected mechanistic divergence among MATE transporters, thereby cautioning against treating them as a single class of molecules during the development of pharmaceuticals for overcoming recalcitrant multidrug resistance.

ONLINE METHODS

Gene cloning and mutagenesis

The gene encoding DinF from *Bacillus halodurans* (DinF-BH) was cloned from genomic DNA (ATCC) into the expression vector pET15b (Novagen). Full length DinF-BH was expressed with a cleavable hexa-histidine tag at the C-terminus. Mutations were introduced

into the *dinF-BH* and *norM-NG* genes in the pET-15b vector using the QuickChange method (Agilent Technologies) and were confirmed by DNA sequencing. *E. coli* BL21 (DE3) Δ*acrAB*Δ*macAB*Δ*yojHI* cells[33] were transformed with pET15b vector containing the inserted genes encoding the DinF-BH and NorM-NG variants. The membrane expression levels of both DinF-BH and NorM-NG were not affected by the single mutations described in the text, as judged by Western blot using an antibody against the His tag.

Drug resistance assay

The drug export activities of DinF-BH and NorM-NG variants were evaluated based on their ability to confer growth resistance to drugs. Drug susceptibility experiments were conducted in Luria-Bertani (LB) medium based on the established protocols[15,34], with each assay repeated at least three times. Briefly, the exponential-phase bacterial culture from freshly transformed cells was diluted to 5×10^5 colony forming unit/ml with LB broth containing isopropyl β-D-1-thiogalactopyranoside (IPTG, 0.1 mM) and ampicilin (100 μg/ml) at each drug concentration. The culture was then incubated at 30°C with shaking and the bacterial growth was monitored after 10 h. Assays were performed in 96-well plates and the attenuance at 600 nm was measured using a microplate reader (Tecan GENios Plus). We defined the minimal inhibitory concentration as the lowest concentration of antimicrobial compounds that precludes growth of *E. coli* under our experimental conditions.

Drug efflux assay

We performed the fluorescence-based transport assays as previously described[8,22], with the following modifications. Briefly, cultures of *E. coli* BL21 (DE3) Δ*acrAB*Δ*macAB*Δ*yojHI* cells expressing DinF-BH or NorM-NG variants were grown at 28°C to an attenuance of ~1.0 at 600 nm. Cells were harvested, washed twice with 100 mM Tris-HCl, pH 7.0, resuspended in the same buffer containing 4.5 μg/ml rhodamine (R6G) and 100 μM carbonyl cyanide *m*-chlorophenyl hydrazone (CCCP), and incubated at 37°C for 15 min. CCCP, an H^+ conductor, was used to deenergize the cell membrane and expedite the accumulation of R6G within the cells. Similar observations were made in the absence of CCCP. To initiate the DinF-BH mediated R6G efflux, 20 mM Citrate-Tris, pH 4.0, or 50 mM diethanolamine (DEA), was added to the sample. To trigger NorM-NG mediated drug efflux, 200 mM NaCl was used. R6G efflux was monitored by measuring the fluorescence with the respective excitation and emission wavelength of 480 nm and 570 nm. Assays were performed in 96-well plates and the fluorescence was measured using a microplate reader (Tecan GENios Plus). The amount of maximum fluorescence was normalized to 1.0 (ref. 8). The R6G efflux activity of each protein was evaluated based on the reduction of R6G fluorescence, which was calculated by subtracting fluorescence in the absence of the artificial cation (H^+ or Na^+) gradient or DEA from that in the presence of the artificial cation gradient or DEA.

Drug-H^+ antiport assay

Everted membrane vesicles were prepared from BL21 (DE3) Δ*acrAB*Δ*macAB*Δ*yojHI* cells expressing DinF-BH variants, NorM-NG or an empty pET-15b vector. Briefly, cells were grown in LB media to an attenuance of 0.5 at 600 nm and induced with 0.5 mM IPTG at 37°C for 3h. Cells were harvested by centrifugation and washed once with buffer containing

10 mM Tris, pH 7.5, 5 mM $MgCl_2$, 0.5 mM DTT and 0.25 M sucrose[24]. The cells were disrupted by using a pre-chilled French press and the cell lysate was centrifuged at 10,000 g for 60 min at 4°C. Membranes were then collected by centrifugation at 100,000 g for 60 min at 4°C. For each measurement, membrane vesicles (100 μg proteins) were added to 2 ml of pre-warmed (30°C) buffer containing 10 mM Tris, pH 7.0, 5 mM $MgCl_2$ and 1 μM acridine orange[24]. The samples were continuously stirred and fluorescence was monitored with an excitation wavelength of 492 nm and emission wavelength of 525 nm using an Olis SLM-8000 spectrofluorometer. Prior to addition of substrates, 2 mM lactate was added to energize the membrane and thereby quench acridine orange fluorescence[24]. Upon addition of 250 μM tetraphenylphosphonium (TPP), fluorescence dequenching occurred due to the extrusion of H^+ by antiporters that move TPP into the everted vesicles across membranes[25]. 5 mM NH_4Cl was finally added to dissipate the H^+ gradient. Similar observations were made when TPP was replaced by dequalinium.

Drug accumulation assay

Cultures of *E. coli* BL21 (DE3) Δ*acrAB*Δ*macAB*Δ*yojHI* cells expressing DinF-BH or NorM-NG were grown at 28°C to an attenuance of ~1.0 at 600 nm (A_{600nm}). Cells were harvested, washed three times with 100 mM Tris-HCl, pH 7.0, resuspended in the same buffer to an A_{600nm} of 1.0/ml. R6G was added to the cells at a final concentration of 4 μg/ml, followed by the addition of 100 mM NaCl or KCl (ref. 8). At each time point, a 1ml-sample was withdrawn, and cells were harvested by centrifugation and washed twice with 100 mM Tris-HCl, pH 7.0. The R6G fluorescence was then measured in the same fashion as specified in the R6G efflux assay. Similar observations were made when R6G was replaced by ethidium.

Protein expression and purification

NorM-NG was expressed and purified as described previously[15]. To express DinF-BH and its mutants, *E. coli* BL21 (DE3) cells were grown in LB media to an attenuance of 0.5 at 600 nm and induced with 0.5 mM IPTG at 37°C for 3h. Cells were harvested by centrifugation and ruptured by multiple passages through a pre-cooled microfluidizer. All the protein purification experiments were carried out at 4°C. Cell membranes were pelleted down by ultracentrifugation and extracted with 1% (wt/vol) n-dodecyl-β-maltoside (DDM, Anatrace) in 20 mM Hepes-NaOH pH7.5, 100 mM NaCl, 20% (vol/vol) glycerol and 1 mM tris(2-carboxyethyl)phosphine (TCEP). The soluble fraction was loaded onto Ni-NTA resin in 20 mM Hepes-NaOH pH7.5, 100 mM NaCl, 20% (vol/vol) glycerol, 0.03% (wt/vol) DDM and 1 mM TCEP. Protein was eluted using the same buffer supplemented with 500 mM imidazole. The protein sample was desalted and incubated with thrombin overnight. After thrombin cleavage the protein sample was desalted and concentrated to ~20 mg/ml before it was further purified by using gel filtration chromatography (Superdex 200) in 20 mM Hepes-NaOH pH7.5, 100 mM NaCl, 10% (vol/vol) glycerol, 0.03% (wt/vol) DDM and 1 mM TCEP. The expression level of DinF-BH appeared to be low, as we routinely obtained less than 10 mg of purified protein from 50 liters of bacterial culture.

Fluorescence polarization assay

The binding of R6G to freshly purified DinF-BH variants was analyzed using the fluorescence polarization assay as previously described[8]. Briefly, the binding experiments were performed using a ligand binding solution containing 20 mM Tris-HCl (pH 8), 50 mM NaCl, 0.03% (wt/vol) DDM, 1 mM TCEP and 1 μM R6G. The protein solution in the same buffer was titrated into the ligand binding solution until the polarization became unchanged. Fluorescence polarization measurements were taken after 10-minute incubations for each protein concentration using an Olis SLM-8000 spectrofluorometer. The excitation and emission wavelengths were 527 and 550 nm, respectively. Data were analyzed using the equation $\Delta FP = FP - FP_{free} = (\Delta FP_{max}\,[protein])/(K_d + [protein])$, where FP is the polarization measured at a given total protein concentration, FP_{free} is the initial polarization of free ligand, ΔFP_{max} is the maximum of polarization change, [protein] is the protein concentration and K_d is the dissociation constant. The titration experiments were repeated three times. To study the effects of pH on the binding of R6G, the fluorescence polarization experiments were performed in the same way as described above for DinF-BH and D40N, except that the pH of the binding solutions varied from 5.5 to 9.0. We analyzed the K_d by fitting it to a competition-based equation: $K_d = (1+ [H^+]/K_i)\,K_{min}$, where K_d is the dissociation constant at any proton concentration, $[H^+]$ is the proton concentration, K_i is the proton inhibition constant, and K_{min} is the limiting (i.e., minimal) dissociation constant[25]. For DinF-BH, the data fitted well whereas for D40N, the K_d was largely independent of $[H^+]$.

Fluorescence measurement of H^+-release

Purified DinF-BH variants and NorM-NG were dialyzed extensively against solutions containing 10% (vol/vol) glycerol, 50 mM NaCl and 0.03% (wt/vol) DDM. For each measurement, protein was diluted to 4 μM in the same buffer supplemented with 2 μM fluoresceine, a pH-sensitive fluorophore that can be used for quantitative measurement of solution acidity[25]. Fluorescence measurement was carried out using excitation and emission wavelengths of 494 nm and 521 nm, respectively. Concentrated TPP was added at the indicated times to reach a concentration of 250 μM, samples (2 ml) were stirred continuously during measurement. Same experiments were repeated three times, which yielded a stoichiometry of 1.00 ± 0.07 H^+ per DinF-BH upon drug binding.

Protein crystallization

Crystallization experiments were performed using the hanging-drop vapor-diffusion method at 22°C. For crystallization, the protein samples (~10 mg/ml) were mixed with equal volume of a crystallization solution containing 100 mM Tris-HCl pH8.5, 100 mM NaCl, 20–30% (vol/vol) PEG400, 0.03% (wt/vol) DDM and 1 mM TCEP. Protein crystals usually appeared within two weeks and continued to grow to full size in a month. For heavy atom derivatization, protein crystals were incubated with 5 mM heavy metal compounds for 8 h at 22 °C. For substrate soaking experiments, protein crystals were incubated with 0.5 mM R6G or tetraphenylarsonium (TPP analog) for 48 h at 22 °C. The R6G-soaked crystals all had a bright reddish color indicative of the bound substrate.

Structure determination and refinement

More than 3,000 crystals were examined at beam-lines 23-ID and 22-ID in Argonne National Laboratory; only a small number (~100) of the crystals were serviceable. X-ray diffraction data were processed using the program suite HKL2000 (ref. 35) and further analyzed using the CCP4 package[36] unless specified otherwise. All structures were solved using a combination of molecular replacement and MIRAS (multiple isomorphous replacement and anomalous scattering) phasing. Initially, a homology model of DinF-BH based upon the structure of NorM-NG[15] was constructed by using the SWISS-MODEL server (http://swissmodel.expasy.org). The homology model was then placed into the unit cell for the apo crystal form by using the program PHASER[37]. Heavy metal binding sites were identified by anomalous difference Fourier analysis and MIRAS phases were subsequently calculated using the program SHARP[38] for the apo and R6G-bound crystal forms. Table 1 listed the optimal subset of derivative data for MIRAS phasing. The resulting electron density maps were further improved by solvent flattening, histogram matching, cross-crystal averaging and phase extension. Both the protruding electron densities for some aromatic amino-acid side-chains and heavy metal binding sites were utilized as markers to aid protein sequence assignment (Supplementary Table 2). Regions of the structures of NorM-NG and NorM-VC were useful as a guide for model building, which was carried out using the program O[39]. Structure refinement (without TLS parameterization) was conducted using the program REFMAC with experimental phases as restraints[40]. No attempts were made to model tetraphenylarsonium or to examine the amino-acid side-chain alterations in DinF-BH upon R6G binding due to the modest resolutions of the data. All structure figures were prepared using the program PyMol (http://www.pymol.org). pKa and electrostatic potentials were calculated using the programs PROPKA[27] and PyMol, respectively. Similar results for pKa prediction were obtained using the H++ web server (http://biophysics.cs.vt.edu).

Supplementary Material

Refer to Web version on PubMed Central for supplementary material.

Acknowledgments

We thank the beam-line staff at 23-ID and 22-ID of Argonne National Laboratory for assistance during data collection. We also thank D. Fu, R. Kaplan, S. Smith, C. Correll and M. Glucksman for comments on the manuscript. This work was supported by the US National Institutes of Health (R01-GM094195 to M.L.) and Rosalind Franklin University of Medicine and Science (M.L.).

References

1. Higgins CF. Multiple molecular mechanisms for multidrug resistance transporters. Nature. 2007; 446:749–757. [PubMed: 17429392]
2. Fischbach MA, Walsh CT. Antibiotics for emerging pathogens. Science. 2009; 325:1089–1093. [PubMed: 19713519]
3. Brown MH, Paulsen IT, Skurray RA. The multidrug efflux protein NorM is a prototype of a new family of transporters. Mol Microbiol. 1999; 31:394–395. [PubMed: 9987140]
4. Omote H, Miasa M, Matsumoto T, Otsuka M, Moroyama Y. The MATE proteins as fundamental transporters of metabolic and xenobiotic organic cations. Trends Pharmacol Sci. 2006; 27:587–593. [PubMed: 16996621]

5. Kuroda T, Tsuchiya T. Multidrug efflux transporters in the MATE family. Biochim Biophys Acta. 2009; 1794:763–768. [PubMed: 19100867]
6. Morita Y, Kataoka A, Shiota S, Mizushima T, Tsuchiya T. NorM of *Vibrio parahaemolyticus* is an Na(+)-driven multidrug efflux pump. J Bacteriol. 2000; 182:6694–6697. [PubMed: 11073914]
7. Chen J, Morita Y, Huda MN, Kuroda T, Mizushima T, Tsuchiya T. VmrA, a member of a novel class of Na(+)-coupled multidrug efflux pumps from *Vibrio parahaemolyticus*. J Bacteriol. 2002; 184:572–576. [PubMed: 11751837]
8. Long F, Rouquette-Loughlin C, Shafer WM, Yu EW. Functional cloning and characterization of the multidrug efflux pumps NorM from *Neisseria gonorrhoeae* and YdhE from *Escherichia coli*. Antimicrob Agents Chemother. 2008; 52:3052–3060. [PubMed: 18591276]
9. He GX, Kuroda T, Mima T, Morita Y, Mizushima T, Tsuchiya T. An H^+-coupled multidrug efflux pump, PmpM, a member of the MATE family of transporters, from *Pseudomonas aeruginosa*. J Bacteriol. 2004; 186:262–265. [PubMed: 14679249]
10. Su XZ, Chen J, Mizushima T, Kuroda T, Tsuchiya T. AbeM, an H^+-coupled *Acinetobacter baumannii* multidrug efflux pump belonging to the MATE family of transporters. Antimicrob Agents Chemother. 2005; 49:4362–4364. [PubMed: 16189122]
11. Li L, He Z, Pandey GK, Tsuchiya T, Luan S. Functional cloning and characterization of a plant efflux carrier for multidrug and heavy metal detoxification. J Biol Chem. 2002; 277:5360–5368. [PubMed: 11739388]
12. Otsuka M, et al. A human transporter protein that mediates the final excretion step for toxic organic cations. Proc Natl Acad Sci USA. 2005; 102:17923–17928. [PubMed: 16330770]
13. Masuda S, et al. Identification and functional characterization of a new human kidney-specific H^+/organic cation antiporter, kidney-specific multidrug and toxin extrusion 2. J Am Sci Nephrol. 2006; 17:2127–2135.
14. He X, et al. Structure of a cation-bound multidrug and toxic compound extrusion transporter. Nature. 2010; 467:991–994. [PubMed: 20861838]
15. Lu M, et al. Structures of a Na^+-coupled, substrate-bound MATE multidrug transporter. Proc Natl Acad Sci USA. 2013; 110:2099–2104. [PubMed: 23341609]
16. Mitchell P. A general theory of membrane transport from studies of bacteria. Nature. 1957; 180:134–136. [PubMed: 13451664]
17. Jardetzky O. Simple allosteric model for membrane pumps. Nature. 1966; 211:969–970. [PubMed: 5968307]
18. Huda MN, Chen J, Morita Y, Kuroda T, Mizushima T, Tsuchiya T. Gene cloning and characterization of VcrM, a Na+-coupled multidrug efflux pump, from *Vibrio cholerae* non-O1. Microbiol Immunol. 2003; 47:419–427. [PubMed: 12906102]
19. Dridi L, Tankoviv J, Petit JC. CdeA of *Clostridium difficile*, a new multidrug efflux transporter of the MATE family. Microb Drug Resist. 2004; 10:191–196. [PubMed: 15383161]
20. Brown DG, Swanson JK, Allen C. The host-induced *Ralstonia solanacearum* genes, *acrA* and *dinF*, encode multidrug efflux pumps and contribute to bacterial wilt virulence. Appl Environ Microbiol. 2007; 73:2777–2786. [PubMed: 17337552]
21. Rodríguez-Beltrán J, Rodríguez-Rojas A, Guelfo JR, Couce A, Blázquez J. The *Escherichia coli* SOS gene dinF protects against oxidative stress and bile salts. PLoS One. 2012; 7:e34791. [PubMed: 22523558]
22. Otsuka M, et al. Identification of essential amino acid residues of the NorM Na^+/multidrug antiporter in Vibrio parahaemolyticus. J Bacteriol. 2005; 187:1552–1558. [PubMed: 15716425]
23. Matsumoto T, Kanamoto T, Otsuka M, Omote H, Moriyama Y. Role of glutamate residues in substrate recognition by human MATE1 polyspecific H^+/organic cation exporter. Am J Physiol Cell Physiol. 2008; 294:C1074–C1078. [PubMed: 18305230]
24. Radchenko MV, Tanaka K, Waditee R, Oshimi S, Matsuzaki Y, Fukuhara M, Kobayashi H, Takabe T, Nakamura T. Potassium/proton antiporter system of Escherichia coli. J Biol Chem. 2006; 281:19822–19829. [PubMed: 16687400]
25. Fluman N, Ryan CM, Whitelegge JP, Bibi E. Dissection of mechanistic principles of a secondary multidrug efflux protein. Mol Cell. 2012; 47:777–787. [PubMed: 22841484]

26. Chen YJ, Pornillos O, Lieu S, Ma C, Chen AP, Chang G. X-ray structure of EmrE supports dual topology model. Proc Natl Acad Sci USA. 2007; 104:18999–19004. [PubMed: 18024586]
27. Bas DC, Rogers DM, Jensen JH. Very fast prediction and rationalization of pKa values for protein-ligand complexes. Proteins. 2008; 73:765–783. [PubMed: 18498103]
28. Adam Y, Tayer N, Rotem D, Schteiber G, Schudiner S. The fast release of sticky protons: kinetics of substrate binding and proton release in a multidrug transporter. Proc Natl Acad Sci USA. 2007; 104:17989–17994. [PubMed: 17984053]
29. Gao X, et al. Mechanism of substrate recognition and transport by an amino acid antiporter. Nature. 2010; 463:828–832. [PubMed: 20090677]
30. Nakashima R, Sakurai K, Yamasaki S, Nishino K, Yamaguchi A. Structures of the multidrug exporter AcrB reveal a proximal multisite drug-binding pocket. Nature. 2011; 480:565–569. [PubMed: 22121023]
31. Perez C, Koshy C, Yildiz O, Ziegler C. Alternating-access mechanism in conformationally asymmetric trimers of the betaine transporter BetP. Nature. 2012; 490:126–130. [PubMed: 22940865]
32. Tanaka Y, et al. Structural basis for the drug extrusion mechanism by a MATE multidrug transporter. Nature. 2013; 496:247–251. [PubMed: 23535598]
33. Yamanaka H, Kobayashi H, Takahashi E, Okamoto K. MacAB is involved in the secretion of Escherichia coli heat-stable enterotoxin II. J Bacteriol. 2008; 190:7693–7698. [PubMed: 18805970]
34. Wiegand I, Hilpert K, Hancock REW. Agar and broth dilution methods to determine the minimal inhibitory concentration (MIC) of antimicrobial substances. Nat Protoc. 2008; 3:163–175. [PubMed: 18274517]
35. Otwinowski Z, Minor W. Processing of X-ray diffraction data collected in oscillation mode. Methods Enzymol. 1997; 276:307–326.
36. Collaborative Computational Project, Number 4. The CCP4 suite: programs for protein crystallography. Acta Crystallogr. 1994; D50:760–763.
37. Read RJ. Pushing the boundaries of molecular replacement with maximum likelihood. Acta Crystallogr. 2001; D57:1373–1382.
38. De La Fortelle E, Bricogne G. Maximum-likelihood heavy-atom parameter refinement for multiple isomorphous replacement and multiwavelength anomalous diffraction methods. Methods Enzymol. 1997; 276:472–494.
39. Jones TA, Zou JY, Cowan SW, Kjeldgaard M. Improved methods for building protein models in electron density maps and the location of errors in these models. Acta Crystallogr. 1991; A47:110–119.
40. Murshudov GN, Vagin AA, Dodson EJ. Refinement of macromolecular structures by the maximum-likelihood method. Acta Crystallogr. 1997; D53:240–255.

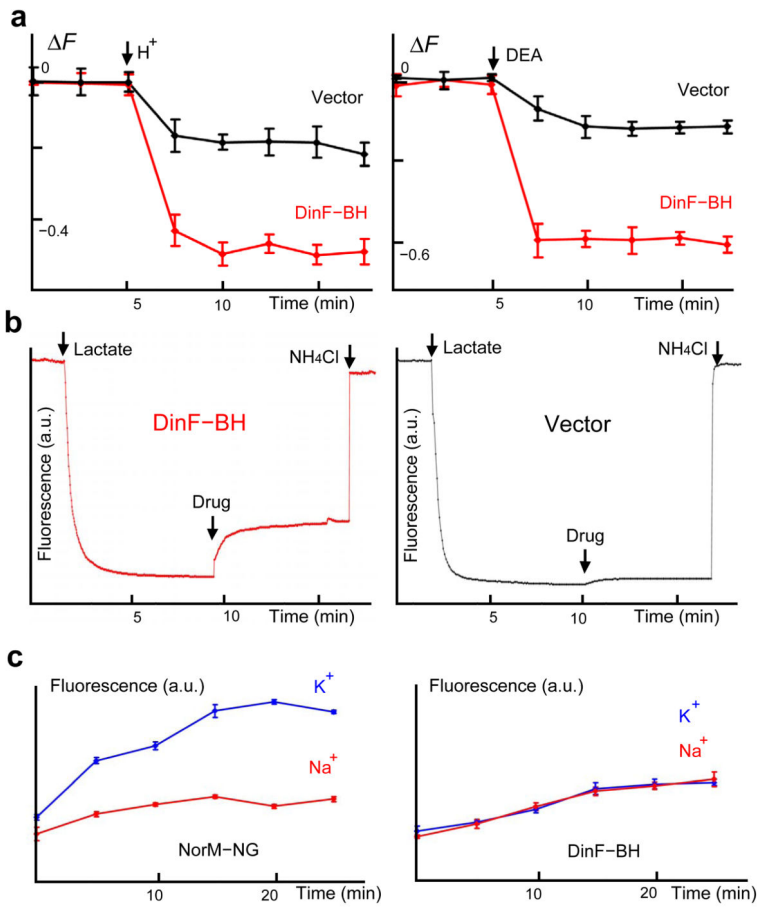

Figure 1.

Functional characterization of DinF-BH. (**a**) Time course of fractional fluorescence reduction (ΔF) as a result of R6G extrusion mediated by DinF-BH (red). Substantially less R6G extrusion was observed in cells containing pET-15b (black). Reactions were initiated by the addition of 20 mM Citrate-Tris, pH 4.0, or 50 mM diethanolamine (DEA). (**b**) TPP-H^+ antiport by everted vesicles containing DinF-BH (red) and pET-15b (black). H^+ movement was monitored by measuring acridine orange fluorescence, which was shown in arbitrary units. (**c**) Cation dependence of R6G accumulation in cells expressing NorM-NG (left) and DinF-BH (right). Time course of R6G accumulation was monitored by measuring the R6G fluorescence after the addition of 100 mM KCl (blue) and NaCl (red). Error bars in (**a**) and (**c**) indicate standard deviations (n=3).

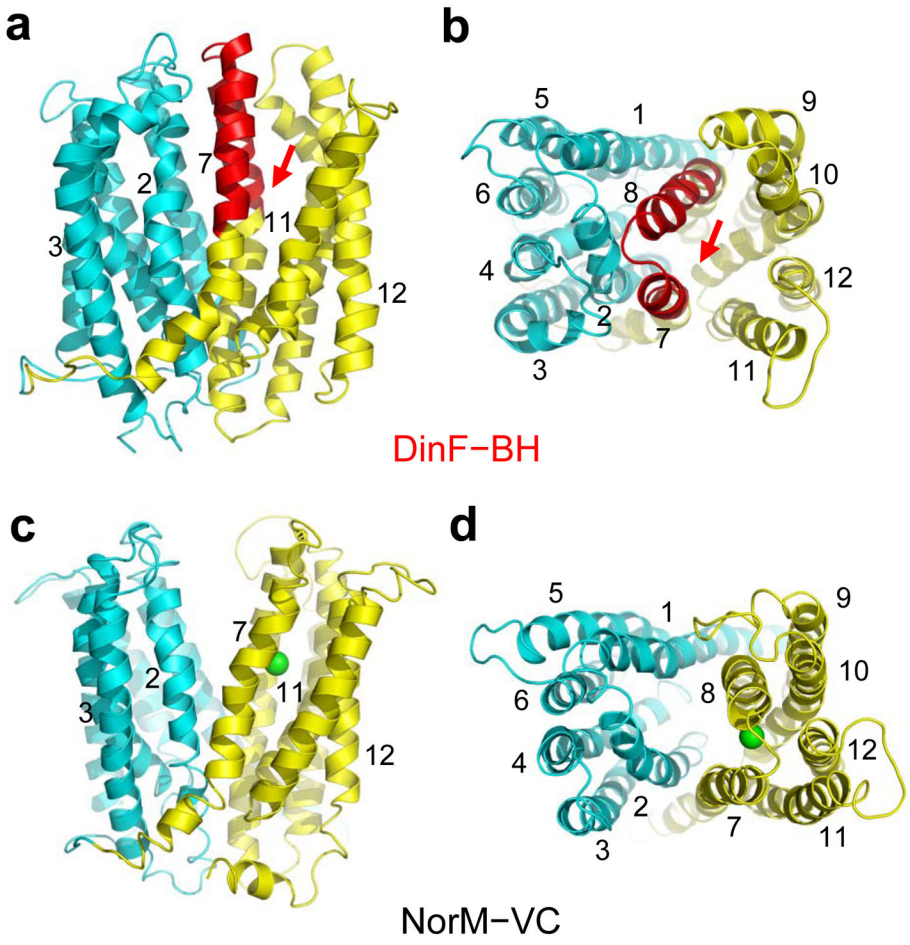

Figure 2.

Structural comparison of DinF-BH and NorM-VC. (**a,b**) Structure of DinF-BH as viewed from the membrane plane (**a**) or the periplasm (**b**). Residues 3–227 and 228–448 were colored cyan and yellow, respectively, except for residues 253–288, which were colored red. Red arrows highlight the solvent-exposed crevice. (**c,d**) Structure of cation-bound NorM-VC (PDB 3MKU)[14] as viewed from the membrane plane (**c**) or the periplasm (**d**). Residues 2–230 and 231–460 were colored cyan and yellow, respectively. Rb^+ (a Na^+ congener) is shown as a green sphere. Relevant transmembrane helices were numbered.

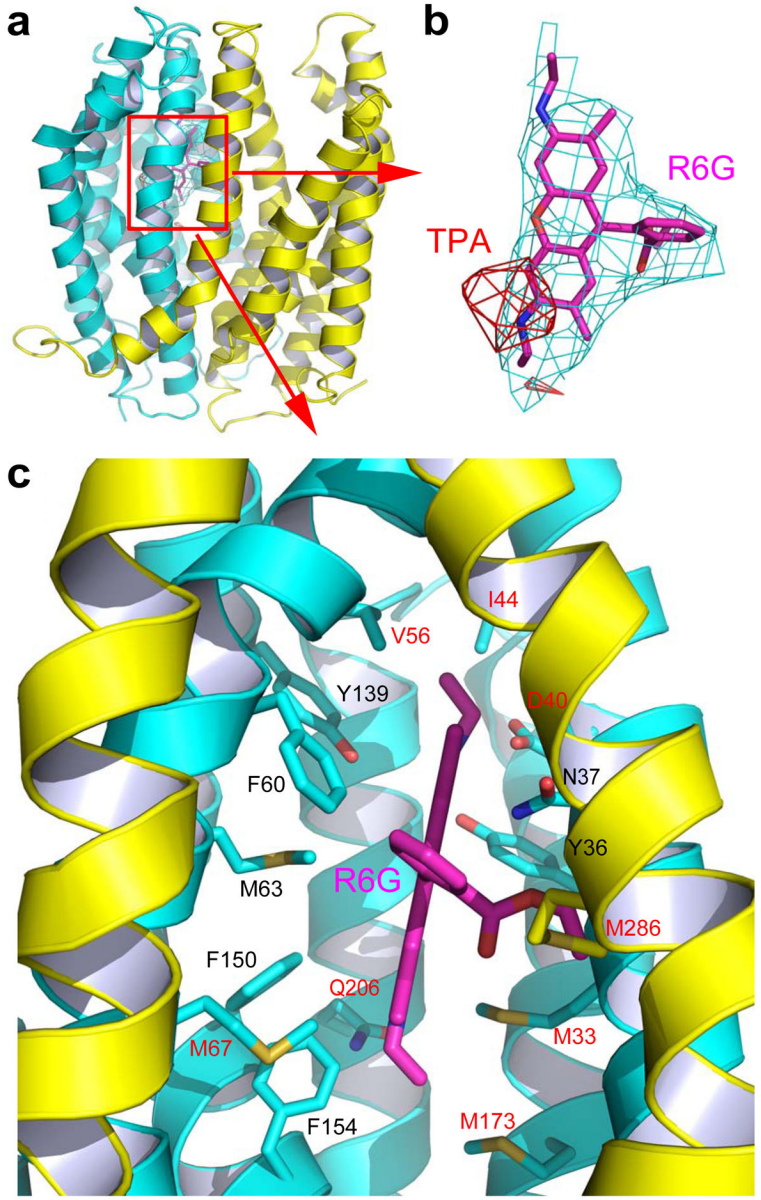

Figure 3.

Structure of the substrate-binding site in DinF-BH. (**a**) DinF-BH is shown in ribbon rendition, with residues 3–227 and 228–448 colored cyan and yellow, respectively. The bound R6G was drawn as magenta sticks. (**b**) Fitting of R6G to the electron density map (cyan mesh), which was calculated to 3.7 Å using solvent-flattened MIRAS phases and contoured at 1.5 σ. Also shown is the difference anomalous Fourier electron density map (red wire) from the substrate tetraphenylarsonium (TPA), which was calculated to 6.0 Å and contoured at 4 σ. Both maps were overlaid onto the final model of R6G (magenta sticks). (**c**) Close-up of the drug-binding chamber, R6G (magenta) and relevant amino acids are displayed in stick representation, with functionally critical residues labeled in red.

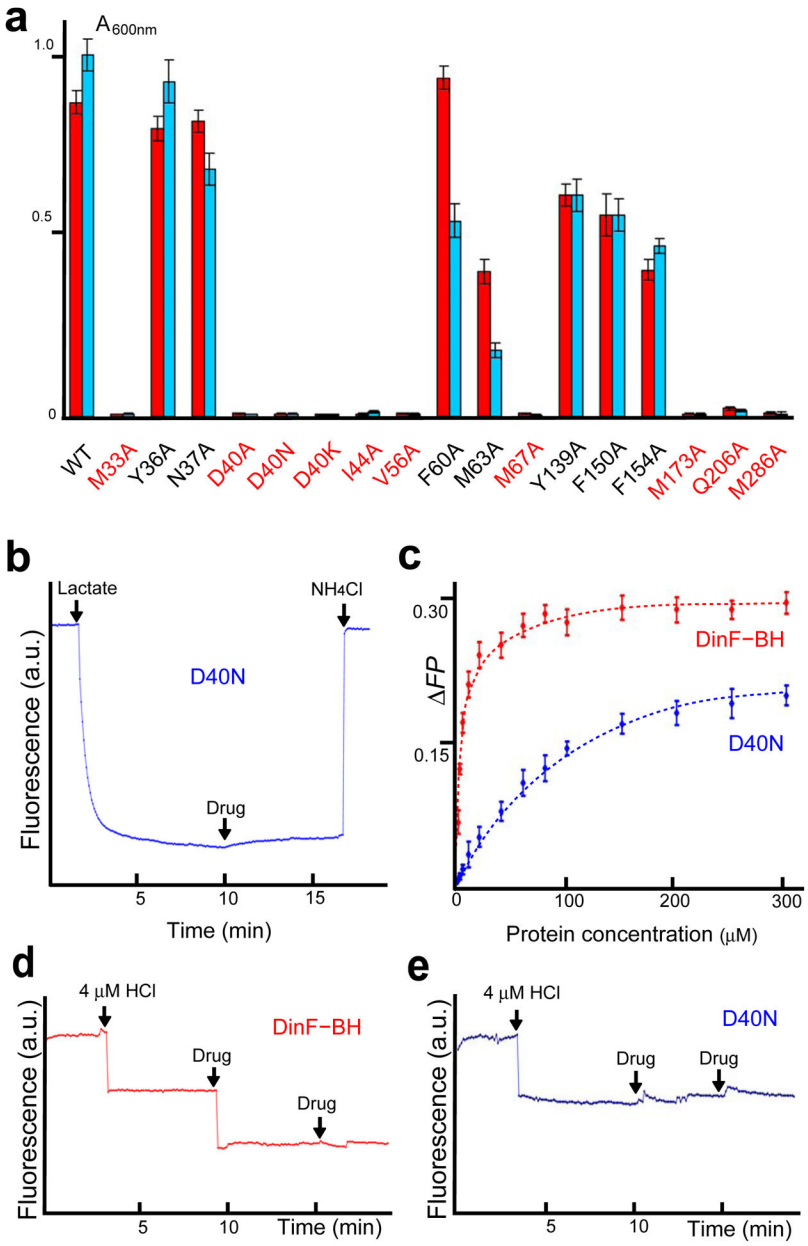

Figure 4.

Functional consequences of mutations in the substrate-binding site. (**a**) Attenuance (A_{600nm}) measurement of bacteria expressing DinF-BH variants in the presence of 0.5 μg/ml ethidium (red) and 3.0 μg/ml R6G (cyan), respectively. (**b**) TPP-H^+ antiport by everted vesicles containing D40N. H^+ movement was followed by measuring acridine orange fluorescence. (**c**) Binding isotherms of DinF-BH (red) and D40N mutant (blue), showing dissociation constants (K_d) of 3.1 ± 0.4 μM and 107.2 ± 4.1 μM, respectively. ΔFP is the increase of fluorescence polarization upon binding of R6G to DinF-BH variants. (**d**) Fluorescence measurement of a solution containing 4 μM DinF-BH. (**e**) Fluorescence measurement of a

solution containing 4 μM D40N, which was unable to release H^+ upon TPP binding. Error bars in (**a**) and (**c**) indicate standard deviations (n=3).

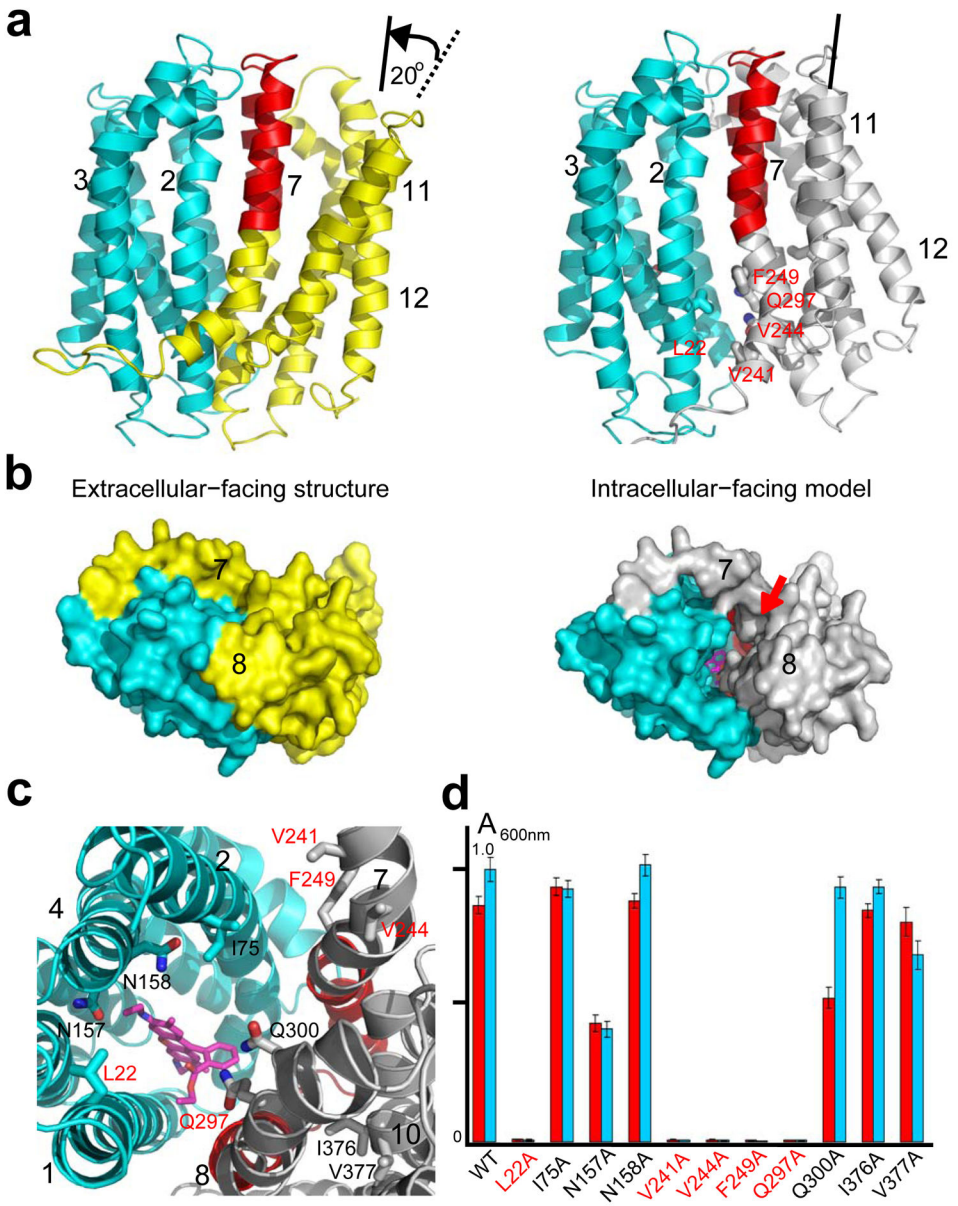

Figure 5.

Modeling intracellular-facing DinF-BH. (**a**) Structures of extracellular- and intracellular-facing DinF-BH as viewed from the membrane. Residues 3–227 were colored cyan, whereas residues 228–448 were colored yellow or gray, except for residues 253–288, which are in red. Black arrow indicates the direction of rotational movement. Dotted and black lines indicate the helical orientations of TM11 before and after the rotation, respectively. Relevant amino acids were drawn as stick models and labeled. (**b**) Surface representations of extracelluar- and intracellular-facing DinF-BH, as viewed from the cytoplasmic side. R6G (magenta) was drawn as a stick model to indicate the substrate-binding site; red arrow highlights the intracellular transport pathway. (**c**) Close-up of the intracellular path as viewed from the cytoplasmic side. R6G (magenta) and relevant amino acids are shown as

stick models. Functionally critical residues were labeled in red. (**d**) The inhibition of bacterial growth as measured by attenuance at 600 nm (A_{600nm}). Bacteria expressing DinF-BH variants were grown in the presence of 0.5 μg/ml ethidium (red) and 3.0 μg/ml R6G (cyan). Error bars represent standard deviations (n=3).

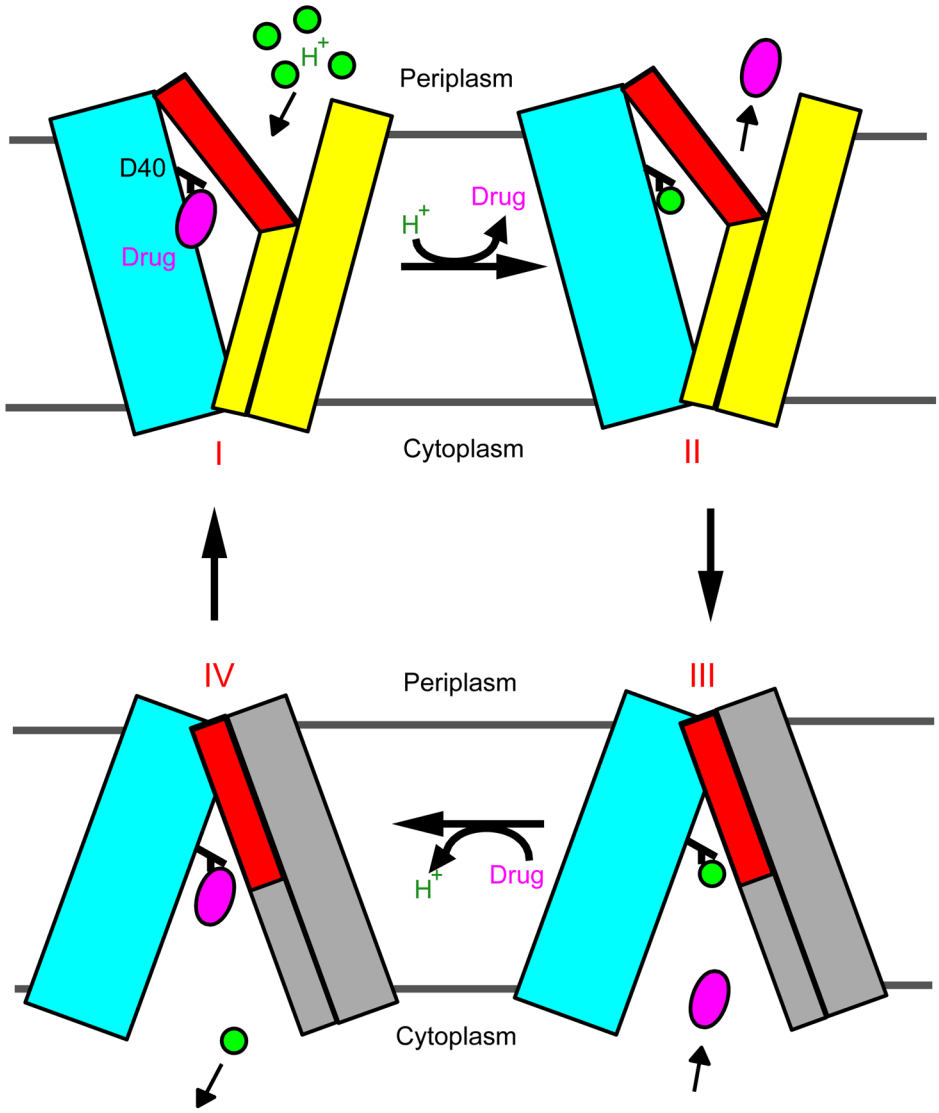

Figure 6.

Proposed transport mechanism for DinF-BH. Bundles of transmembrane helices were drawn as rectangles, with TM1-TM6 colored cyan, TM7-TM8 red (extracellular halves) and yellow or gray (intracellular portions), and TM9-TM12 yellow or gray. Drug and proton were drawn as a magenta oval and a green circle, respectively. D40 was colored and labeled in black. During transport, protonation of D40 in extracellular-facing, drug-bound DinF-BH (state I) triggers drug release. The protonated, extracellular-facing DinF-BH (state II) then switches to the protonated, intracellular-facing state (III) by undergoing a rotational movement as described in the text. Drug binding to DinF-BH from the cytoplasm subsequently promotes the deprotonation of D40 and yields the drug-bound, intracellular-facing state (IV), which eventually returns to the drug-bound, extracellular-facing state (I).

Table 1

Data collection, phasing and refinement statistics for apo DinF-BH

	Native	EMTS[a]	TMLA[a]	$K_2Pt(NO_2)_4$	Orange Pt[a]	$KAu(CN)_2$	EMTS[a] $KAu(CN)_2$	$KAu(CN)_2$ $K_2Pt(NO_2)_4$
Data collection								
Space group	$P2_12_12_1$	$P2_12_12_1$	$P2_12_12_1$	$P2_12_12_1$	$P2_12_12_1$	$P2_12_12_1$	$P2_12_12_1$	$P2_12_12_1$
Cell dimensions								
a, *b*, *c* (Å)	90.8, 95.1, 101.7	91.5, 93.8, 103.5	89.7,93.7, 101.9	89.0, 94.0, 102.8	88.7,92.2, 101.8	90.2, 93.7, 101.9	92.7, 93.7, 105.2	92.2, 94.4, 104.8
α, *β*, *γ* (°)								
Resolution (Å)	60–3.2 (3.3–3.2)[b]	60–4.0 (4.2–4.0)	60–4.5 (4.8–4.5)	60–4.7 (5.0–4.7)	60–4.5 (4.8–4.5)	60–4.0 (4.2–4.0)	60–4.5 (4.8–4.5)	60–4.5 (4.8–4.5)
R_{sym} or R_{merge}	0.05 (0.53)	0.08 (0.78)	0.10 (0.58)	0.13 (0.99)	0.08 (0.54)	0.06 (0.39)	0.08 (0.53)	0.07 (0.49)
$I/\sigma I$	58.5 (2.1)	51.2 (1.8)	47.2 (4.8)	29.3 (2.0)	34.6 (2.1)	23.1 (1.9)	49.9 (2.2)	36.3 (2.3)
Completeness (%)	97.3 (92.2)	98.4 (91.1)	99.1 (91.2)	98.4 (88.5)	93.5 (64.7)	89.8 (59.7)	98.4 (93.5)	95.6 (80.3)
Redundancy	15.0 (8.9)	13.4 (6.9)	13.5 (6.7)	6.4 (4.1)	11.3 (6.7)	5.0 (3.4)	17.7 (10.1)	11.8 (6.3)
Refinement								
Resolution (Å)	3.2							
No. reflections	14129							
R_{work}/R_{free}	0.284/0.306							
No. atoms								
Protein	3413							
Ligand/ion Water								
B factors								
Protein	172							
Ligand/ion Water								
r.m.s deviations								
Bond lengths (Å)	0.011							
Bond angles (°)	2.0							

[a] EMTS: thimerosal. TMLA: trimethyllead acetate. Orange Pt: chloro (2,2′:6′,2″-terpyridine) platinum (II) chloride.

[b] Values in parentheses are for highest-resolution shell.

Table 2

Data collection, phasing and refinement statistics for ligand-bound DinF-BH

	R6G	R6G EMTS[a]	R6G TMLA[a]	R6G $K_2Pt(NO_2)_4$	TPA[a]
Data collection					
Space group	$P2_12_12_1$	$P2_12_12_1$	$P2_12_12_1$	$P2_12_12_1$	$P2_12_12_1$
Cell dimensions					
a, *b*, *c* (Å)	90.2, 93.9, 102.3	91.9, 94.5, 103.7	92.1,93.9, 104.1	91.2, 94.4, 102.4	90.3,94.3, 103.6
α, *β*, *γ* (°)					
Resolution (Å)	60–3.7 (3.8–3.7)[b]	60–4.2 (4.4–4.2)	60–4.6 (4.9–4.6)	60–4.6 (4.9–4.6)	60–4.2 (4.4–4.2)
R_{sym} or R_{merge}	0.06 (0.54)	0.08 (0.54)	0.09 (0.54)	0.09 (0.45)	0.07 (0.55)
$I/\sigma I$	39.6 (2.0)	50.7 (1.6)	56.7 (2.5)	54.6 (2.1)	68.8 (2.6)
Completeness (%)	94.9 (73.7)	96.2 (75.5)	96.3 (68.3)	95.6 (64.1)	98.3 (89.7)
Redundancy	15.7 (7.3)	27.0 (10.5)	28.6 (14.7)	21.6 (14.1)	37.1 (19.7)
Refinement					
Resolution (Å)	3.7				
No. reflections	8797				
R_{work}/R_{free}	0.287/0.301				
No. atoms					
Protein	3413				
Ligand/ion Water	33				
B factors					
Protein	202				
Ligand/ion Water	280				
r.m.s deviations					
Bond lengths (Å)	0.011				
Bond angles (°)	2.1				

[a] EMTS: thimerosal. TMLA: trimethyllead acetate. TPA: tetraphenylarsonium (TPP analog).

[b] Values in parentheses are for highest-resolution shell.